Polymer 267 (2023) 125674

Contents lists available at ScienceDirect

Polymer

journal homepage: www.elsevier.com/locate/polymer

Rigid composite bio-based polyurethane foams: From synthesis to LCA analysis

Federica Recupido [a,1], Giuseppe C. Lama [a,1], Mario Ammendola [a], Ferdinando De Luca Bossa [a,b], Andrea Minigher [c], Pietro Campaner [c], Angela Gala Morena [d], Tzanko Tzanov [d], Mariana Ornelas [e], Ana Barros [e], Filipa Gomes [e], Veronica Bouça [e], Regina Malgueiro [e], Monica Sanchez [f], Eva Martinez [f], Luigi Sorrentino [a], Laura Boggioni [g], Massimo Perucca [h], Sridhar Anegalla [h], Roberta Marzella [a], Pierluigi Moimare [g], Letizia Verdolotti [a,*]

[a] Institute of Polymers, Composites and Biomaterials (IPCB), National Research Council, P.le E. Fermi 1, 80055, Portici, Italy
[b] Department of Chemistry, Center for Macromolecular Engineering, Carnegie Mellon University, 4400 Fifth Avenue, 15213, Pittsburgh, PA, USA
[c] AEP Polymers Srl, 34149, Basovizza, Italy
[d] Group of Molecular and Industrial Biotechnology, Chemical Engineering Department, Universitat Politècnica de Catalunya, Rambla Sant Nebridi 22, 08222, Terrassa, Spain
[e] CeNTI – Centre for Nanotechnology and Smart Materials, R. Fernando Mesquita 2785, 4760-034, Vila Nova de Famalicão, Portugal
[f] ACCIONA, Avda. de Europa, 18. Parque Empresarial La Moraleja, 28108, Alcobendas, Spain
[g] Institute for Chemical Science and Technologies, CNR, Via Alfonso Corti 12, 20133, Milan, Italy
[h] Projecthub360, Corso Laghi 22, 10051, Avigliana, Italy

ARTICLE INFO

Keywords:
Functionalized hemp powders
Nanosilica
Composite bio-based polyurethane foams
Mechanical performances
Fire resistance
LCA analysis

ABSTRACT

This paper provides a bio-based polyurethane foam (PUR) solution, following a cradle-to-factory approach. The design of bio-based rigid PURs, reinforced with sustainable fillers have gained remarkable attention in "*green*" construction sector. Their marked performances make them a viable solution for synthetic counterparts' replacement. In this work, functionalized hemp fibers and silica powders were selected as reactive fillers, imparting multifunctional properties to the designed PURs. Hemp fibers underwent ultramilling, phenolation and/or nano-transformation to obtain four different filler types, i.e. nano- and micro-sized hemp particles, and functionalized hemp nano and micro-size couples. Silica nanoparticles were extracted from rice husk and functionalized with phytic acid. The composite PURs were prepared by adding 6 % wt of filler to cardanol/vegetable-based polyol solutions. The effect of the filler's chemistry on the properties of the foams was investigated. A Life Cycle Assessment of the filler production stages was performed to assess their eco-profile impact.

1. Introduction

The depletion of resources from fossil origin, the accumulation of non-degradable plastics in the environment and their impact on the climate change are the focus of several international forums. All of them agree on the paramount importance to reduce the use of plastics from fossil origin, which global production reached around 360 million tons in 2018 [1,2]. Instead, bioplastic materials, derived from bio-based or biodegradable polymers, account for less than 1% of the worldwide plastic production [2]. Synthetic polyurethanes rank 6th among all fossil-based polymers with a production of around 22 million tons per year [2,3] and a global market of $50 billion (2016). The polyurethane market is usually categorized in foams (65%, comprising 60% flexible foams and 40% rigid foams), coatings (13%), elastomers (12%), adhesives (7%) and others (3%) [1,3,4].

Polyurethane foams (PURs) are generally obtained by poly-addition reaction between polyols, isocyanates and suitable blowing agents. Several additives (catalysts, surfactant and flame retardants) are added in order to tune the final characteristics of the product [1]. The mechanical and functional properties of the foams are strongly affected by the nature of polyols and isocyanate precursors as well as by the distribution of the soft and hard segments of PURs [1,3,5].

* Corresponding author.
E-mail address: letizia.verdolotti@cnr.it (L. Verdolotti).
[1] These authors contributed equally to this work.

https://doi.org/10.1016/j.polymer.2023.125674
Received 21 July 2022; Received in revised form 30 December 2022; Accepted 2 January 2023
Available online 8 January 2023

Nowadays, the use of bio-based polyols is largely investigated with the purpose to provide sustainable alternatives to conventional crude oil-derivatives [5,6] in applications such as thermal and acoustic insulation [7,8] or automotive [9,10]. A common approach is to select bio-based polyols, from either vegetable origin or biomass-based-products, such as lignin or cellulose [1,11–13], and to partially or totally replace the conventional ones [7]. However, bio-based PUR foams, having mechanical, functional and flame retardancy performance comparable to or beyond the conventional PUR foams, usually require the addition of fillers. In this regard, bio-based fillers such as silica and hemp fibers or powders (i.e. lignocellulosic residues) have gained attention due to their low cost and wide availability [11].

Silica particles can be obtained from agricultural waste, e.g. rice husk, with high purity and yield. Rice husk is largely available and is used for different applications, such as drug delivery, catalysis [14], energy storage [15], construction material [16,17], and the production of value-added ceramics [18]. Different methods are available for the extraction of silica from rice husk. Among them, the acid leaching of husk followed by thermal treatment at high temperatures (>500 °C) is one of the simplest and most efficient ways to obtain silica nanoparticles (SiO_2 NPs). Such particles proved to be effective in improving the tensile strength of epoxy-based composites [19]. Further surface modification of the silica particles endows them with enhanced functional properties. For instance, thermal stability is achieved by surface modification of silica particles with phytic acid (PA).

PA is a bio-based and environmentally friendly compound that has been used to improve the flame retardancy of different polymeric matrices [20]. Several works reported on the use of this compound for the modification of silica particles by means of tetraethyl orthosilicate (TEOS) as precursor. Cheng et al. reported on the use of PA-modified silica particles to impart durable flame retardancy to wool fabric [21], and Sui and co-workers developed core-shell Ni@SiO_2-PA nanoparticles that were incorporated into an epoxy resin, improving its thermal stability [22].

Hemp (*Cannabis Sativa* L.*)* has been extensively used throughout history as a source for fabrics, food, and medicine [23]. Different parts of the plant are currently used for industrial applications, including stalk for obtaining fibers and hempseeds for extracting vegetal oil. During the cold-press process for producing hempseed oil, a hemp press cake by-product is generated, which represents more than half of the initial hemp mass. Due to the large amounts of protein (20–50%) and fibers (20–30%) [24], hemp press cake has been considered as a potential nutritional additive for human consumption [25,26], although it is actually only used as animal feedstock. The high content of aliphatic and phenolic hydroxyl groups, as well as amino groups, makes possible the chemical modification of hemp to impart specific functionalities, such as fire resistance, or for increasing its reactivity. Enzymatic functionalization is an environmentally friendly approach to improve the performance of hemp fibers in specific applications. Moreover, the transformation of biomass residues into nano-sized fillers for improving the mechanical performance of composite materials has been pursued.

In this framework, and with the aim of fulfilling the EU directives for Circular Economy concerning the reduction of the production of plastic materials form oil resources, this paper presents a comprehensive design, characterization and analysis of new bio-based composite foams, containing five different fillers derived from hemp and silica powder, as well as two bio-based polyols for PUR formulation. The fillers studied in this work enable the synthesis of novel bio-based PUR foams that comply with the foams' functionalities and safety requirements. The mechanical, thermal, fire resistance and chemical properties of such systems have been investigated. Specifically, the effects of size, as well as functionalization, of hemp and modified nano-sized silica particles have been assessed. The selected natural fillers were added to the polyurethane matrix at 6 wt % (this amount was optimized in previous study [11]), observing a significative improvement of both thermal and mechanical properties of the obtained foams.

However, the mere use of bio-based raw materials and of renewable source (e.g. biomass) could not be enough to assure a complete sustainability or a lower environmental impact of the products. Only a holistic approach, including all life cycle steps and all possible impacts, may avoid the generation of environmental damages and side effects, even after replacing an oil-based matrix with a bio-based one. For this reason, the evaluation of the sustainability of the chemical processes, either considering novel chemical routes for renewable sources or optimizing well-established processes, is crucial. For this purpose, the Life Cycle Assessment (LCA) methodology was applied in accordance with ISO 14040–14044 standards [27,28]. The analysis was based on a comprehensive mass-energy balance, according to the "cradle-to-gate" perspective, which takes into account all impacts - from materials and energy sources to the fillers production stage. In accordance with the above-reported ISOs, the four basic analysis phases were implemented: Goal and Scope Definition, Life Cycle Inventory Analysis (LCI), Life Cycle Impact Assessment (LCIA) and Interpretation [29].

2. Experimental

2.1. Chemicals

Cashew nutshell liquid (CNSL) based polyol, GX9104 (OH value: 245 mg KOH/g oil) was supplied by Cardolite Corporation (Bristol, PA, USA). Mannich-based polyol RV020010 (OH-value equal to 270 mg KOH/g), was provided by AEP Polymers (Trieste, Italy). Niax PM 40 and CH_3COOK, used as catalysts for blowing and polymerization reactions, respectively, and Niax L5388 and Niax L6900, the silicone copolymers used as cell stabilizers, were provided by Momentive s.r.l. (Italy). Distilled water (H_2O) and n-pentane (Sigma Aldrich (Italy) were used as blowing agents. Lactic acid ($CH_3CH(OH)CO_2H$ and DABCO® 100 BA, used to improve the cream time, and the tris (2-chloroisopropyl)-phosphate (TCPP) flame retardant were supplied by Evonik (Italy). MDI (methylene diphenyl isocyanate) (SUPRASEC 2085), having 31.5% NCO-content, was purchased from Huntsman S.r.l. (Italy).

For the preparation of silica nanoparticles (SiO_2_PA) rice husk purchased from Álvaro Alves Borges, Lda (Figueira da Foz, Portugal) was used as a silica source. Hydrochloric acid (HCl) 37 wt % (Fisher Chemicals) and phytic acid solution (50% w/w aqueous solution) from Sigma-Aldrich were used for surface functionalization.

Hemp protein residues obtained from oil-pressing process of hempseeds were kindly provided by Kroppenstedter Ölmühle (Germany). The dried press cake was milled before use. Tannic acid and 3′,5′-dimethoxy-4′-hydroxyacetophenone (acetosyringone) was provided by ACROS Organics (Belgium). Bradford reagent (Coomasie Brilliant Blue G), and Folin-Ciocalteu phenol reagent were purchased from Sigma Aldrich. Novozym 51003 laccase enzyme from *Myceliophthora thermophila* (EC 1.10.3.2) with activity of 1322 U/mL (defined as the amount of enzyme converting 1 μmol ABTS (2,2′-azino-bis (3-etilbenzotiazolin-6-sulfonic acid) to its cation radical (ε_{436} = 29 300 M^{-1} cm^{-1}) in 0.05 M sodium acetate buffer pH 5 at 25 °C), was supplied by Novozymes (Spain) [30,31].

Conventional polyisocyanurate (PIR) panels, alternatively covered with glass fibers (GF) skin, or in bare skin (NGF), were supplied by DANOSA (Spain) and used as reference foams for flammability test, having comparable thickness and thermal conductivity of that of the examined PUR foams.

2.2. Filler preparation and functionalization and polyurethane foams synthesis

The procedures related to the preparation and functionalization of fillers are reported in Sections 1.1 and 1.2 of Supplementary Materials. A two steps method was used to synthesize the bio-based foams. First, a solution (*Component A*) of all the additives (catalysts, silicone

surfactants, flame retardant and blowing agents) and the polyols blend (GX9104 and RV020010) was prepared in a beaker. To this mixture, 6 wt % of the selected fillers was added and mixed in an ultrasonic bath for 50 min to assure a complete dispersion of the filler in *Component A*. Subsequently, MDI (*Component B*) was added to *Component A* at a fixed ratio (NCO/OH = 1.5).

The obtained mixture was stirred for 20 s at 500 rpm and then poured in a rectangular closed mold (20 cm × 30 cm x 5 cm), previously pre-heated at 55 °C. The obtained composite PURs were cured for 3 h at 60 °C. A pristine PUR (i.e. without fillers) was also produced as reference foam. The composition of the composite bio-foams in part by weight (pbw), where total pbw of polyols was 100, is reported in Table 1.

The obtained PUR foams are denoted as following: PUR pristine (foam with no filler), PUR_nH (foam reinforced with hemp nanoparticles), PUR_ph_nH (foam reinforced with phenolated hemp nanoparticles), PUR_μH (foam reinforced with hemp microparticles), PUR_ph_ μH (PUR reinforced with phenolated hemp microparticles) and PUR_SiO_2 (foam reinforced with silica nanoparticles), respectively.

In all studied cases, quantification of the renewable material content within the polyurethane foams was determined using a sustainability index (as described in Ref. [11] named as S.I.), defined as the ratio between renewable materials (coming from vegetable oils as well as biomass sources or agricultural wastes and so forth) and the total foam mass (equation (1)):

$$\text{S.I.} = 100 \bullet \frac{S.P.}{T.W.} \quad (1)$$

where S.P. is the mass of sustainable materials, T.W. is the total mass of the foam.

Sustainable indexes of 45 wt % and about 50 wt %, for pristine and composite foams, respectively, were defined.

2.3. Fillers and bio-foams characterizations

2.3.1. Wettability and size distribution of fillers

To evaluate the fillers' dispersibility in the polyol mixture, wettability analysis was performed through contact angle measurements [32]. Filler powders were compressed by means of a tablet press (Silfradent s. r.l., Italy) with the aim of creating a uniform solid surface. Subsequently, the sessile droplet technique was carried out, controlled by a commercial software (OCA 25, Data Physics Instruments GmbH, Berlin, Germany), to estimate the static contact angle on the flat sample surface. Droplets of 1 μL were gently dispensed by a microliter syringe. Millipore water and polyol-based mixture (containing all the components, except n-pentane and MDI) were used as wetting agents. Six measurements were performed for each test. Particle size distribution and phenolic content were determined through Dynamic Light Scattering (DLS) and spectroscopic techniques. Information is shown in Section 1.3 (supplementary materials).

2.3.2. FTIR analysis of fillers and bio-PURs

Fillers and composite PURs were analyzed by Attenuated Total Reflectance Fourier transform infrared spectroscopy (FTIR-ATR). To detect the main functional groups of the fillers and the occurring polymerization reaction of PURs, a FTIR PerkinElmer Spectrum 100 Series spectrophotometer (Waltham, MA, USA) with a spectral range from 4000 to 650 cm^{-1}, resolution factor of 8 cm^{-1} and averaging 64-scans, was used. Regarding PUR foams, FTIR spectra were collected on the surface of the cubic foam sample, in the region between 1400 and 1800 cm^{-1}, prior background correction [1,8,9,33,34].

2.3.3. Thermal degradation, thermal conductivity and flammability investigations

The thermal degradation of PURs was evaluated by thermogravimetric analysis (TGA) and derivative thermogravimetric analyses (DTGA) both under nitrogen (N_2) (volumetric flow rate = 40 mL min^{-1}) and in air flows (volumetric flow rate = 50 mL min^{-1}). A Q500 (TA Instruments, New Castle, DE, USA) instrument was used. The tests were carried on approximately 10 mg of samples, at a heating rate equal to 10 °C/min in the temperature range from 30 °C to 700 °C. Thermal conductivity, λ, was also measured according to EN12667 [34].

To assess the flame retardancy behavior of selected composite foams, two different fire tests were considered: the first test according to ISO 11925–2:2020 [34-37] and the second one ISO 5660–1:2002 [36], where foam properties were compared with those of commercial PIRs. All details related to the first configuration are reported in Section 2.1 of supplementary materials.

In the second case, the fire properties were quantitatively estimated through exposure to radiant heat by using an oxygen consumption cone calorimeter (Fire Testing Technology, Tecnalia, Spain; Fig. S1, supplementary materials). Specimen of 100 × 100 mm and thickness of 50 mm pre-conditioned to constant mass (at a temperature of 23 ± 2 °C and relative humidity 50 ± 5%) were exposed to an external heat flux set at 25 kW/m^2. Three specimens for each composition were tested. The following parameters were measured: heat release rate (HRR in kW/m^2, representing the amount of energy released as heat per unit area by a specimen during the combustion, which takes into account fire growth, smoke emission and toxic gases, time to ignition (TTI in s), peak heat release rate (pHRR, kW/m^2), fire performance index, FPI (which corresponds to the ratio of TTI/pHRR in s• m^2/kW) and the total heat release (THR, kJ/m^2), respectively.

2.3.4. Morphological analysis

To analyze the morphology of polyurethane foams, a scanning

Table 1
Composition of the composite PUR foams.

Components	PUR_pristine (pbw)	PUR_nH (pbw)	PUR_ph_nH (pbw)	PUR_μH (pbw)	PUR_ph_μH (pbw)	PUR_SiO_2 (pbw)
Component A						
GX9104	50	50	50	50	50	50
RV020010	50	50	50	50	50	50
NIAX PM 40	0.5	0.53	0.53	0.53	0.53	0.53
CH3COOK	0.5	0.53	0.53	0.53	0.53	0.53
NIAX L5348	0.5	0.53	0.53	0.53	0.53	0.53
NIAX L6900	0.5	0.53	0.53	0.53	0.53	0.53
LACTIC ACID	14.9	13.2	13.2	13.2	13.2	13.2
TCPP	10	9.0	9.0	9.0	9.0	9.0
DABCO®100 BA	0.3	0.26	0.26	0.26	0.26	0.26
H_2O	0.7	1.3	1.3	1.3	1.3	1.3
N-PENTANE	1.5	2.7	2.7	2.7	2.7	2.7
FILLER*	–	15.6	15.6	15.6	15.6	15.6
Component B						
MDI	128.6	121.4	121.4	121.4	121.4	121.4
Sustainability index (%)	45	49.2	48.4	49.2	49.2	49.1

electron microscope (FEI ESEM Quanta 200 FEG scanning electron microscope Eindhoven, The Netherlands) was used. Samples (0.5 cm × 0.5cm × 0.1 cm) were cut from PURs in the foam growth direction. Before imaging, specimens were sputter coated with gold-palladium layer by means of a Emitech K575X sputter coater. Images were acquired by setting 30 kV acceleration voltage and different magnifications were used. Cell size distribution and average cell size were evaluated by means of a Java-implemented open-source imaging software (Image J).

2.3.5. Compression and impact analysis

The compressive response of PURs up to 70% strain was identified according to the ASTM D1621 standard [37] and carried out using a universal testing machine (model CMT4304 from Shenzhen SANS Testing Machine Co. China), equipped with a 30 kN load cell and operated at a 5 mm/min cross-head displacement rate. Specimen (5.5 x 5.5 × 5 cm^3) were cut from foams panels [38].

The density of PUR foams was measured as the ratio between mass and volume. An analytical balance (model AB265-S from Mettler Toledo, Columbus, OH, USA) was used to measure the sample mass. For each tested condition, foam density is reported as average and standard deviation of at least 4 different independent measurements.

The obtained mechanical results were carefully analyzed, and the specific strength was evaluated for each material, by dividing the obtained compressive strength (σ) by the corresponding density (ρ). This ratio is widely used in literature, especially in the field of composite foams, in order to better understand the mechanical behavior of the studied foam, once modified (by means of a filler intercalation or a coating formation) [39–42].

Impact tests were performed by using a falling dart impact testing machine (model Fractovis Plus, CEAST, Pianezza –Turin, Italy) with a circular impact head (50 mm in diameter). Specimen dimensions were 20 x 20 × 10 mm (length x width x height). Low velocity impact tests were performed at 20 °C after conditioning the samples for 60 min. The impact energy was 1.2 J, and the impact velocity was set equal to 1 m/s.

2.3.5.1. Modified Gibson-Ashby model. The results of mechanical and density characterization were correlated to the cellular morphology of the foams. To this end, a modified Gibson-Ashby model of a closed cell foam was used [38,43]. By a correlation between the relative density (ratio between the apparent density of the foam, ρ, and the density of the solid matrix, ρ_s) and the relative elastic modulus (Young's modulus of the foam, E, divided by the Young's modulus of the solid matrix, E_s), the model can give an insight on how the foam behaves from a structural point of view at the micro-scale. The mathematical representation of the standard model stands in the following equation:

$$\left(\frac{E}{E_s}\right) = C\varphi^2\left(\frac{\rho}{\rho_S}\right)^2 + C'(1-\varphi)\left(\frac{\rho}{\rho_s}\right) \tag{2}$$

where E/E_s is the relative modulus, ρ/ρ_s is the relative density, C and C′ are two constants of proportionality, and the factor φ is the volume fraction of the polymeric matrix located in cell edges. For $\varphi = 1$, the equation degenerates into:

$$\left(\frac{E}{E_s}\right) = C\left(\frac{\rho}{\rho_S}\right)^2 \tag{3}$$

which models the linear elastic behavior of an open-cell foam.

However, a more general equation can give an idea of how the cells constituting the foam structure are made [38]:

$$\left(\frac{E}{E_s}\right) = C\left(\frac{\rho}{\rho_S}\right)^n \tag{4}$$

Here we propose a new equation, for a hybrid open/closed cells structure:

$$\left(\frac{E}{E_s}\right) = C\varphi^2\left(\frac{\rho}{\rho_S}\right)^n + C'(1-\varphi)\left(\frac{\rho}{\rho_s}\right) \tag{5}$$

which correlates the mechanical behavior of the porous structure by means of a non-integer exponent *n*. This equation makes possible to estimate how the composite matrix is distributed among edges and walls of the pores.

2.3.6. Life Cycle Assessment (LCA)

The goal of the present Life Cycle Assessment study was to identify the potential environmental impacts of both production and functionalization methods for both hemp and silica fillers employed in the composite bio-based PUR investigated solutions. The functional unit of 5.9 g of filler preparation was considered, which corresponds to the reference mass employed in the foam formulation. The "cradle-to-gate" approach was applied to the investigation of the functional system, whose boundaries encompassed the whole process from bio-based raw material sourcing and extraction to fillers functionalization. A dedicated system modelling included both background (e.g., source production of rice husk and hemp press cake) and foreground (e.g., extraction, activation, neutralization and functionalization) processes. All details related to the primary Life Cycle Inventory (LCI) data and the life cycle impact assessment (LCIA [44]) are reported hereafter.

The LCI database Ecoinvent v3.7 was employed to enable the life cycle impact assessment (LCIA), literature data were also employed to develop reference models to fill the gap of missing datasets in Ecoinvent v3.7 databases and to overcome its data limitations. For the available processes, regionalized datasets were considered, whereas Europe datasets were associated to the developed models.

The Life Cycle Impact Assessment (LCIA) was performed by using OpenLCA v1.10 software and the CML 2001 impact method providing a comprehensive environmental assessment with eleven impact categories and associated unit of measurements, including: Abiotic depletion (ADP: kg Sb eq), Abiotic depletion (fossil fuels) (ADP-f: MJ), Acidification (AP: kg SO_2 eq), Eutrophication (EP: kg PO_4 eq), Fresh water aquatic ecotoxicity (FAETP: kg 1,4-DB eq), Global warming (GWP100a) (GWP: kg CO_2 eq), Human toxicity (HTTP: kg 1,4-DB eq), Marine aquatic ecotoxicity (MAETP: kg 1,4-DB eq), Ozone layer depletion (ODP: kg CFC-11 eq), Photochemical oxidation (POCP: kg C_2H_4 eq), Terrestrial ecotoxicity (TETP: kg 1,4-DB eq). The study used these eleven environmental impact categories to characterize the environmental profile including local and global impact parameters as well as toxicological parameters.

3. Results and discussion

3.1. Fillers characterization

3.1.1. FTIR and wettability analysis

FTIR spectra of fillers are reported in Fig. S2 (Supplementary materials). Hemp-based powders showed the typical bands of polysaccharides at 1150 cm^{-1}, which are largely present in hemp, associated to the C–O–C stretching vibrations. The absorption bands at 2930 and 2850 cm^{-1} correspond to the symmetrical and asymmetrical C–H stretching of the methyl and methylene groups of polysaccharides, respectively. The peak at 3430 cm^{-1} was attributed to the overlapping N–H and O–H vibration of functional groups of hemp particles [45]. SiO_2 particles (both functionalized and non-functionalized ones) exhibited bands at 802 and 1059 cm^{-1}, which could be assigned to asymmetric stretching vibration of Si–O–Si bonds [32–34,46]. For the Si–OH particles, there was also a broad band at 3430 cm^{-1}, attributed to OH vibration [45,47]. This band was not present for SiO_2 nanoparticles, where all the absorbed water was removed during the final stage of the extraction process. The PA spectrum displayed a broad band at 2114-2480 cm^{-1} corresponding to the OH and P═O groups [47–49]. This band was also visible on the SiO_2_PA spectrum, confirming the

presence of PA on the surface of the SiO_2_NPs.

Wettability analysis (Fig. S3, supplementary materials) revealed that hemp powders presented a good capability to interact with both water and polyol mixture This could be ascribed to the presence of high amount of –OH groups on their surface.

3.2. Bio-foams characterization

3.2.1. FTIR characterization

FTIR analysis of the bio-based PUR foams is reported in Fig. S4 and discussed in Section 3.2 (Supplementary Materials).

3.2.2. Thermogravimetric, thermal conductivity and flammability analysis

The thermal degradation behavior of produced foams was performed in N_2 (Fig. 1a) and air flow (Fig. 1b). Temperatures at three different degradation stages (weight loss at 5, 20 and 50%) were evaluated, together with the residual mass at 700 °C, under both N_2 and air flows (Tables S1a and S1b respectively). The abovementioned weight loss percentages corresponded to three specific degradation stages as previously reported in Refs. [8,11,45], where the maxima of the weight loss derivative function could be recorded. The first degradation stage referred to the removal of low molecular weight molecules (such as H_2O or chemically bonded water in the filler) that generally occurs in the range between 150 and 250 °C. The second degradation stage, occurring in the range between 250 and 350 °C, corresponded mainly to the breakage of urethane linkages, and of the polyol chain, with the formation of volatile molecules such as CO_2, amines and carbodiimide (produced by dimerization of isocyanate molecules). Further degradation occurred at higher temperatures, as a result of the breaking of more thermally stable bonds, such as the aromatic rings, present in the isocyanate, in the Mannich polyol, and in the carbodiimide [11,50]. Finally, a residue of char and of the ceramic inorganic filler was detected at 700 °C in N_2 atmosphere, while the residue at 700 °C under air flow was only correlated to the inorganic filler, and no char was present.

Under inert gas flow, the nano-enabled composite bio-PURs presented slightly higher degradation temperatures with respect to pristine bio-PUR. The nano-composite bio-PURs showed a residual mass at 700 °C, higher than that of the unfilled system. Among functionalized hemp-based PUR foams, the highest thermal stability was detected in PUR_ph_nH and PUR_ph_μH. However, it should be noted that nano and micro-sized hemp particles did not result in different thermal degradation performances. The highest thermal stability was exhibited by PUR_SiO_2, which showed the highest residual mass at 700 °C (18.2%, Fig. 1a, Table S1a), despite the fact that the degradation temperatures were comparable to those of PUR reinforced with hemp particles.

This result can be related to the particularly effective protection induced by the phytic acid treatment on silica particles, which translated into the ability to develop a protective and dense char during the thermal degradation process on the polyurethane matrix [46,47].

PUR_SiO_2 showed the highest thermal stability also under air flow. In particular, the highest degradation temperature (462 °C) at 50% weight loss was detected (Fig. 1b, Table S1b), with a residual weight of about 6.8% at 700 °C. This was surely due to the inorganic nature of the filler, which might enhance the fire resistance of the material because the residual mass acted like a barrier layer which reduced the flame propagation during combustion [11,34,45,48,49,51]. Under air flow, the effect of hemp powders on the thermal stability of foams was not significant, since degradation temperatures at the three stages were almost comparable to those of the pristine PUR, and no residual traces were detected at 700 °C.

The thermal conductivity (λ) was also performed with the aim of identifying the effect of the fillers on the heat conduction capability. A significant contribution to the flame retardance performance of a material is related to its capability to reduce the heat transfer. Pristine and composite PURs behaved in a very similar way, showing a λ value around 33 mW/(m K) (Table 2). This is in agreement with comparable filled-foamed systems reported in literature [11,34]. It is also significant because it demonstrates that the presence of the fillers did not deteriorate the insulating capability of the foam.

For the flammability analysis, PUR_nH and PUR_ph_nH foams were not included, as shrinkage effects were noticed after foaming. Results concerning the ISO 11925–2:2020, through which, PUR flammability properties were qualitatively investigated, are discussed in Section 2.3 of supplementary materials.

HRR (Heat Release Rate) curves of the PURs and PIRs are reported in Fig. 2. Enlargements of HRR curves at short ignition time are presented as inset. The HRR curve of the examined PIRs (with and without glass fibers) was characterized by a sharp peak, as the whole sample was pyrolyzed at the same time [52–54]. PIRs ignited immediately with a rapid increase in the HRR value and then rapidly decay [55–57].

Table 2
Thermal conductivity of the selected PUR foams.

SAMPLE	λ (mW/m·K)
PUR-Pristine	33.4 ± 0.2
PUR_nH	33.8 ± 0.1
PUR ph_nH	33.1 ± 0.1
PUR μH	34.1 ± 0.8
PUR ph_μH	33.4 ± 0.5
PUR_SiO_2	32.9 ± 0.4

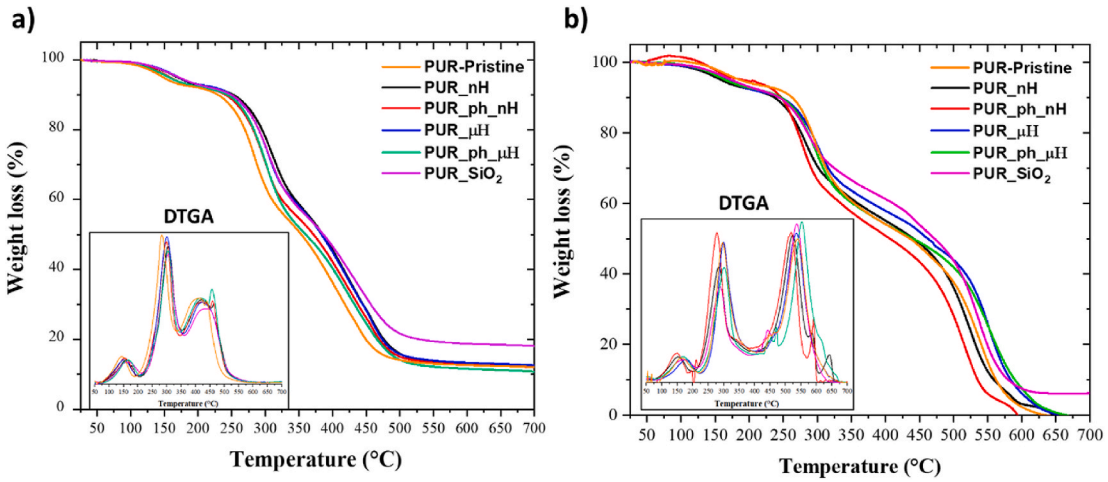

Fig. 1. Thermogravimetric analysis of PUR foams reinforced with the examined fillers: a) in N_2 and b) in air flows, respectively.

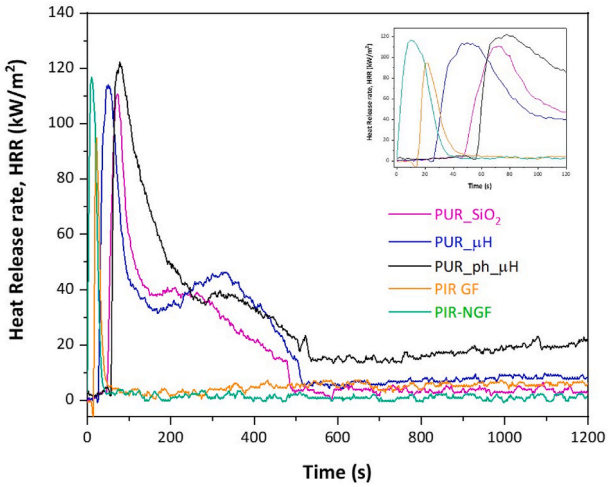

Fig. 2. Heat Release Rate evolution over time for the examined composite PUR foams. A comparison with the reference polyisocyanurate products was performed with and without glass fibers (GF-PIR and NGF PIR). Inset: enlargements of HRR curves at short ignition time.

Composite PURs exhibited the "*thermally thick charring*" curve, in which an initial increase of HRR was observed until a char layer formation was generated, which acted as flame propagation barrier and had a beneficial effect on fire safety [57–59] mainly for the PUR_SiO_2, where, the presence of functionalized silica particles [59] catalyzed the carbonization of the polymeric surface, forming a thermally stable and dense protective char layer.

The time to ignition, TTI (Fig. 2, Table S2, supporting materials) was remarkably delayed in the composite foams (38s for PUR_μH, 54.5s and 54 s respectively for PUR_ph_μH and PUR_SiO_2). Such behavior could be ascribed to the capability of functionalized fillers to promote the flame propagation and to reduce the development of smoke into the PUR matrix as reported in Refs. [60,61].

Furthermore, to determine the material fire safety, the Total Heat Release (THR) and the potential "*flashover*" (i.e. fire performance index FPI, Table S2, supporting materials) were evaluated and discussed. In details, the total heat release values of PIRs (4.7 MJ/m^2 for PIR-GF and 3.85 MJ/m^2 for PIR-NGF, respectively) were one order of magnitude lower than those exhibited by the composite foams, where the highest value was attained for the case of phenolated hemp-reinforced foam (THR equal to 38.5 ± 4.9 MJ/m^2). Even if in the early stages of a fire exposition, the behavior of PIR and PUR was similar, at larger ignition time, the trimers present in the PIR molecular structure, which is known to form a stable and thicker char layer, seemed not to be able to resist to the flame propagation, while the composite-PUR foams did. Additionally, the fire performance index, FPI, of the obtained foams were found to be comparable or higher than those of the conventional PIRs.

3.2.3. Morphological analysis

SEM images (Fig. 3a) were acquired perpendicularly to the foam growth direction (Fig. 3b). For each cell, an ellipse was traced on each cell to take into account their irregular shape. The cell size was obtained as average between the major and minor axes traced on that cell.

PUR foams presented closed cells, with very thin walls in all studied cases. Pristine PUR exhibited a homogenous cell structure with an average cell size of 500 ± 87 μm, which is typical of rigid PUR foams [11,33,45,60]. The addition of the filler affected the cell size as well as cells' interconnections. Specifically, hemp fillers resulted in more elongated and irregular cell shape with respect to the pristine PUR, as also reported elsewhere [62,63]. The presence of the filler indeed affects the kinetic reaction of the foam and consequently the cellular structure. The reaction rate is related to the initial temperature and to the presence of the filler, which also acts as a nucleation site as reported elsewhere

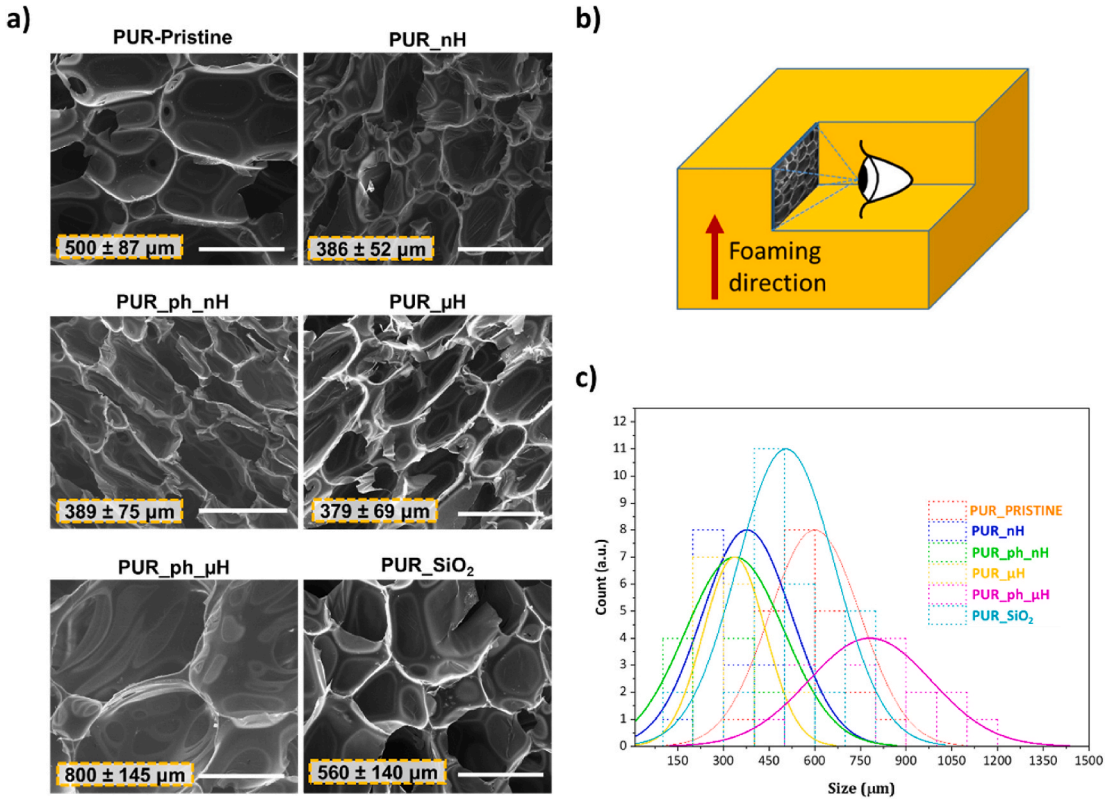

Fig. 3. a) SEM microphotographs of the obtained PUR foams. 200× magnification, scale bar = 500 μm. b) Representation of the direction of observation for SEM analysis. c) Cell size distribution of the obtained PUR foams.

[34,63,64]. During the blowing reaction of PUR, when the developed gas exceeds the solubility limit, and when diffusion into existing bubbles is not fast enough, more nucleation sites are formed. The formation of smaller cells is further promoted by the presence of dispersed particles. The cell size of non-functionalized hemp nanoparticles filled composite foams (PUR_nH and PUR_μH) was similar. Particle phenolation led to different morphological features for micro- and nano-sized hemp particles. More specifically, elongated and larger cells were obtained in presence of phenolated hemp microparticles (PUR_ph_ μH with average size of 800 ± 145 μm, Fig. 2c), probably resulting from particles agglomeration during the foaming process, whereas smaller cells were attained in presence of phenolated hemp nanoparticles (Fig. 2c, PUR_ph_nH, 389 ± 76 μm). The dispersion of SiO_2_PA particles within the polyurethane mixture (PUR_SiO_2) generated spherical cells, with an average size (586 ± 140 μm) comparable to the pristine PU foam but with a wider size distribution.

3.2.4. Compression and impact investigation

Compression tests were performed along the foam growth direction, while the impact characterization was performed on selected samples cut orthogonally with respect to the foam growth direction. The scope of this choice is to evaluate the relevant mechanical properties according to the loading conditions occurring during the installation of the panels or their service life, when small impacts might occur on the large surface of panels. The main static loading is typically carried by the panels along the vertical direction. The representative element and the testing directions, with respect to the foaming direction and to the installation positioning, is depicted in Fig. 4a.

Pristine PUR exhibited the lowest elastic region (up to yield strength, Fig. 4b) among all systems, with PUR_μH showing the steepest slope at small strain [33,34,65,66]. PUR_ph_nH and PUR_μH showed an elastic-plastic curve shape, since, right after the linear elasticity of the first trait, the curve presents a maximum followed by a plastic yielding [65–68]. All other systems showed no maximum after the linear elastic region, and directly reported a plateau. The composite foams exhibited higher values, in terms of compression modulus (E) and strength at 10% strain (σ_{10}) (Table 3). For PUR_ph_nH and PUR_μH, σ_{10} was evaluated at the strength peak, which generally occurs for values of strain lower than 10%. In addition, the density of hemp-based composites was lower than that of the pristine PU foam, hence the specific performances were even better. The presence of functionalized silica particles in PUR_SiO_2 resulted in a foam with higher density, leading in the reduced specific performance of that system.

The impact behavior of composite materials is usually reduced by the presence of particles/polymer interfaces, which promote the formation and propagation of cracks. The force versus time curves (dashed lines in Fig. 4c), recorded during the impact tests, showed an initial steep increase of the load (in accordance with the compressive modulus of the foam), followed by a strength plateau and a peak. This latter stage corresponded to the densification of the foam and occurred for all

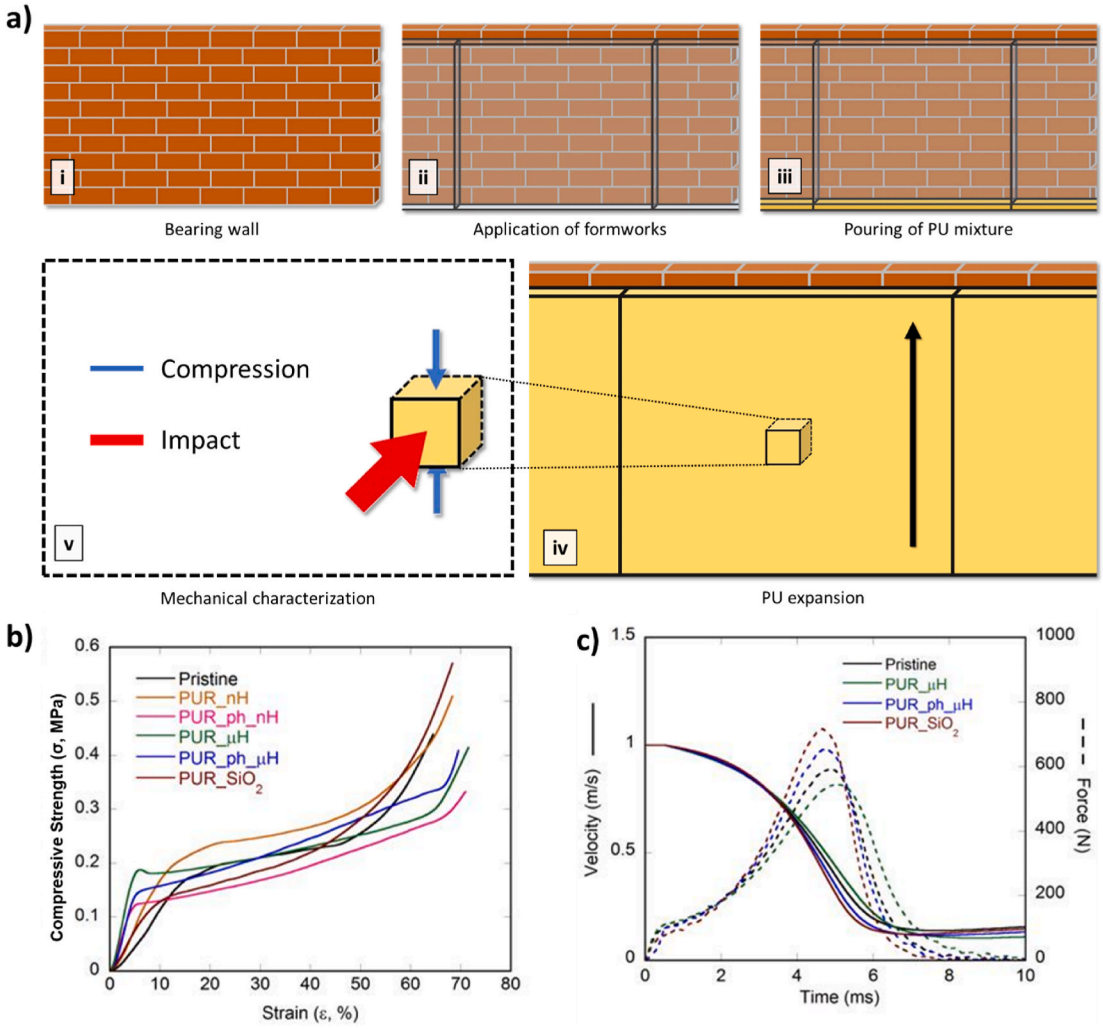

Fig. 4. a) Schematization of installation of rigid PUR foam panels on a building wall along with the representation of impact and compression loads. b) Strength vs strain curves for the obtained PUR foams. c) Dart velocity and impact force curves in time for the obtained PUR foams.

Table 3
Elastic modulus, compressive strength at 10% of deformation, density and the normalized Strength with respect to density at 10% of deformation of the investigated PUR foams. Data are reported as average and standard deviation of 4 independent measurements.

SAMPLE	Modulus (E) (MPa)	Strength @ ε = 10% (σ_{10}) (MPa)	Density (ρ) (kg/m^3)	*S*-Strength @ ε = 10% (σ_{10}[a]) (MPa/kg/m^3)[b]
PUR Pristine	1.05 ± 0.35	0.10 ± 0.02	63.9 ± 0.3	1.59
PUR_nH	2.00 ± 0.14	0.17 ± 0.03	53.3 ± 2.2	3.12
PUR_ph_nH	3.15 ± 0.17	(0.14 ± 0.02)[a]	50.0 ± 1.8	2.70
PUR_μH	4.53 ± 0.35	(0.21 ± 0.02)[a]	49.9 ± 0.8	4.16
PUR_ph_μH	3.80 ± 0.30	0.16 ± 0.01	59.6 ± 1.6	2.61
PUR_SiO$_2$	1.90 ± 0.29	0.13 ± 0.01	68.1 ± 3.6	1.89

[a] These values were taken in correspondence of the maximum value reached by σ before the deformation was at 10% (@ASTM-D1621)
[b] Specific Strength: *S*-Strength.

samples at 80% strain. It is remarkable that, despite the increased stiffness showed by the filled foam compositions, their impact performance was not depleted by the presence of reinforcing particles and all systems were still able to withstand the same high-speed load of the pristine PUR foam, as demonstrated by the similar impact velocity curves (solid lines in Fig. 4c).

3.2.5. *Modified Gibson-Ashby model*

The modified Gibson-Ashby model, where the relative elastic modulus is reported as a function of the relative density (Eq. (5)), allows a direct interpretation of the results by correlating the mechanical properties with the morphological parameters of the cellular structure (Fig. 5).

$$\left(\frac{E}{E_s}\right) = C\varphi^2\left(\frac{\rho}{\rho_S}\right)^n + C'(1-\varphi)\left(\frac{\rho}{\rho_s}\right) \quad (5)$$

As first step, equation (4) was used to determine C and C′ for each set of material. Averaged values of relative density and relative modulus were used by alternatively imposing φ = 1 and φ = 0 as boundary conditions. Such values were then averaged to calculate the general values of C and C', which were equal to 0.84 and 0.04, respectively. The exponent *n* was identified by means of equation [4], setting C = 1 (Table 4). As a final step, specific φ values for each system were identified determined by means of Eq. (5), by considering φ as a variable. Absolute values of the solution φ (Table 4) gave an insight of how the composite matrix was actually distributed among the cell edges and walls. More specifically, the model allowed to discriminate how much stress is applied to cell edges and walls through two parameters, namely edge bending (EB) and face stretching (FS). The presence of different fillers gave different results, in terms of φ, mostly depending on the shape and on the surface chemistry of the filler itself (see the SEM micrographs shown in Fig. S6 of Supplementary Materials).

Pristine foam had the highest φ values (0.88), with EB almost twice the value of FS, meaning that most of the applied stress was held by cell edges. Instead, in composite foams, the results were the opposite, since FS values were higher than EB ones. As a main outcome, it can be assessed that the reinforcing effect of fillers resulted to be better exploited when dispersed in cell walls rather than on the edges. For example, in PUR_SiO$_2$ edges occupied a higher volume (φ = 0.61), but FS is higher than EB. Despite the presence of modified silica particles in both edges and walls, the presence of silica in the walls allowed to bear the most of the load.

In PUR_SiO$_2$, the peculiar surface chemistry of the NPs improved the load bearing. The functionalization had, in fact, reduced the tendency of the NPs to agglomerate, thus making them more compatible with the polymeric matrix, and, therefore, better dispersed in edges and walls. PUR_nH and PUR_ph_nH, where unmodified and modified hemp nanoparticles were used, respectively, confirmed the previous hypothesis. In fact, PUR_nH showed a lower compressive modulus (−33%) with respect to PUR_ph_nH, but FS was similar, indicating that a clear advantage was induced by the increased compatibility of particle surfaces.

The use of micro-sized particles led to different results. PUR_μH and PUR_ph_μH, where unmodified and modified hemp microparticles were used, respectively, exhibited the highest values of compressive modulus, with PUR_ μH slightly prominent. Also in this case the modified particle surface in PUR_ph_μH resulted in EB lower than FS. Nevertheless, PUR_μH showed a lower FS with respect to PUR_ph_μH, as a result of the different particle distribution in the structural elements of the porous structure.

The comparison of compressive strengths showed a significantly improved performance of composite foams with respect to pristine PUR foams. In particular, σ_{10} resulted to be from 26% (PUR_SiO$_2$) to 104% higher (PUR_ph_μH), while the specific strength (σ_{10}*) was from 20% (PUR_SiO$_2$) to 162% higher (PUR_ph_μH), with respect to the pristine PUR values.

This normalization of the mechanical properties against density allowed to incontrovertibly determine the enhancement of the mechanical strength associated to the presence of hemp-based fillers, which was strongly influenced by their size and surface chemistry.

3.2.6. *Life Cycle Assessment (LCA)*

In order to allow a direct comparison among the environmental

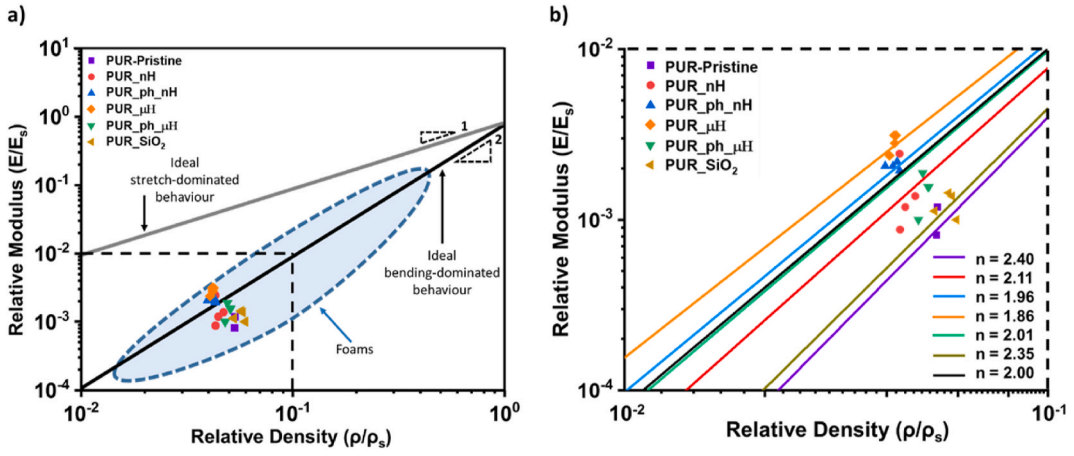

Fig. 5. Graphical representation of the modified Gibson-Ashby model. a) Relative elastic compressive modulus as a function of relative density for each tested PUR foam is compared with data shown in Ref. [51]. b) Enlargement of the inset in a), where n parameter is illustrated for each tested material.

Table 4
Parameters of the Gibson-Ashby's model for each tested PUR foam.

SAMPLE	*r*Density[a] (−)	*r*Modulus[a] (−)	C (φ = 1 in Eq. [2])	C' (φ = 0 in Eq. [2])	n (−)	φ (−)	Edge bending (EB, %)	Face stretching (FS, %)
PUR_Pristine	0.053	0.001	0.31	0.02	2.40	0.80	64.6	35.4
PUR_nH	0.044	0.001	0.70	0.03	2.11	0.21	7.8	92.2
PUR_ph_nH	0.042	0.002	1.13	0.05	1.96	0.20	3.8	96.2
PUR_µH	0.042	0.003	1.55	0.07	1.86	0.43	18.8	81.2
PUR_ph_ µH	0.050	0.002	0.96	0.05	2.01	0.21	4.2	95.8
PUR_SiO_2	0.057	0.001	0.37	0.02	2.3	0.64	31.6	68.4

[a] Relative density: *r*Density, Relative Modulus: *r*Modulus.

profiles [27–29] referred to the five composite systems, all values in each impact categories (ICs) are referred to the highest one among the filler options. Fig. 6 shows the modulation of the obtained results and provides the fillers sustainability ranking that may be obtained by setting the order relation associated to each ICs. Indeed, the almost self-similar pattern that allows obtaining the same ranking in all IC unambiguously identifies the best and the worst cases. In Table S3 of Supplementary Materials, the data related to each impact category are reported.

The main contribution to the fillers production impacts was represented by the preparation and functionalization steps. This was mainly due to two factors. The first was associated to the renewable nature of the bio-based fillers source, while, the second was connected to the high specific direct energy requirement for preparation and functionalization associated with the current fillers production at lab scale.

The considered fillers within the same source had two different sizes and property-oriented usage. The differences among the first four fillers solutions (hemp particles) were associated to the particles size (particles at nano scale displayed the larger impact due to the sonication process) and to the extra phenolation process required to get phenolated nano-sized hemp and phenolated micro-sized hemp (particles subject to phenolation display enhanced impacts). The highest impacts in all ICs were shown by silica functionalization with phytic acid (SiO_2).

The Carbon Footprint (CFP) followed the same ranking w.r.t. of the other ICs and was represented by the GWP impact category expressed in kg CO_2 eq for all the reference samples (nH at 1.23, ph_nH at 3.57, µH at 0.02, ph_µH at 0.54, SiO_2 at 8.70). SiO_2 displayed the highest relative impact when compared to other fillers (more than double the impact of the phenolated n-Hemp) and ph_nH and nH felt next to it. It is worth to note that, the nano-sized hemp provided a larger impact with respect to phenolated micro-sized hemp, showing how the top-down process to obtain nano sized fillers determining a considerably higher environmental impact.

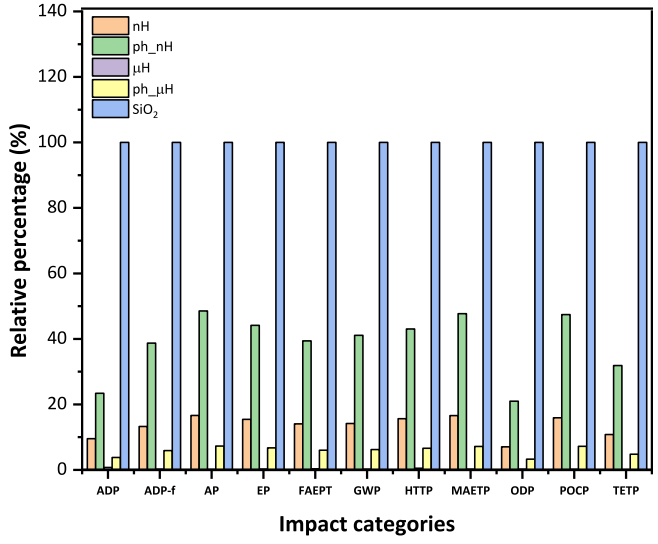

Fig. 6. Comparison of relative impact categories of five different fillers: nHemp, phenolated nHemp, µHemp, phenolated µHemp, PA-SiO_2.

A further consideration related to the application of the LCA methodology extended to the whole product [67] life cycle suggests that, to balance the larger impact in the production stage, the enhanced technical properties associated with the particle size reduction down to nanoscale and with the NPs functionalization by phenolation, should determine a considerable impact reduction during their service in order to render the functionalized NPs a viable solution. For this reason, the environmental impact assessment referred to the specific main technical material functionality of each investigated solution is advisable.

Furthermore, another relevant point is that, the assessed impacts referred to lab scale processes; future industrial scaled-up processes should be more energy efficient, allowing a reduction of wastes in the synthesis stage, and it could be optimized to determine a reduced environmental burden. The evaluation of environmental impacts with the quantitative based LCA methodology extended to the whole bio based composite foams products will allow the identification of hotspots and opportunities to minimize the product environmental impacts for all the impact categories considered along the product life cycle.

4. Conclusions

In this work, composite rigid bio-based polyurethane foams were synthesized and extensively characterized in terms of thermal, mechanical and flammability properties. Organic (hemp) and inorganic (silica) fillers underwent specific functionalization processes (i.e. phenolation and/or size reduction) to formulate rigid composite PUR foams. The selected fillers showed different chemical interactions within PUR mixture and led composite PUR materials to have distinct structural and functional properties. More specifically, the use of phytic acid-functionalized silica particles (inorganic filler) resulted in composite foams with reduced thermal degradation and improved fire resistance, with the highest mass residual at 700 °C (18.2%) and TRR value 5-fold higher than those of conventional PIR panels.

On the other hand, hemp particles-based composite PUR foams exhibited the best mechanical performances, with a compressive strength of 0.2 MPa, in the case of hemp nanoparticles. This might be related to a significant reduction in the cell size, as demonstrated by the morphological analysis and the Gibson-Ashby model. The phenolation treatment had no significant effect on the final PUR characteristics, except for the case of flammability analysis, where phenolated hemp-reinforced foams presented higher ignition time and higher TRR (about 4-fold higher than that of conventional PIR panels).

The comparative LCA assessment, applied to materials and processes developed in the present work, showed some critical points. LCA results were referred to lab scale synthesis and functionalization processes, therefore the assessment conclusions can be largely improved. Nevertheless, the obtained results already provided relevant indications for materials and processes selection and optimization, and to identify their associated environmental burdens. A comprehensive analysis involving all the material life cycle stages is needed to support final decisions, since initial higher impacts may turn in lower global impacts, providing that, the technical performance of the composite systems during their service could determine overall environmental impact reductions. As a

future perspective of this work, new functionalization routes could be considered in order to improve the filler's compatibility and dispersibility into the PUR matrix. To this end, a combination of different fillers (functionalized or unfunctionalized ones and with different size) might be potentially designated to improve functional (i.e. insulating properties) and mechanical properties of the composite PUR foams. Moreover new functionalized fillers having remarkable self-retardancy characteristics can be considered with the goal to reduce the use of petrol-based flame retardant components.

Funding

This research was funded by EU (Horizon 2020/BBI-JU Topic: BBI. 2017.D5, Type of action: BBI-IA-DEMO, REINVENT project, Proposal number: 792049).

CRediT authorship contribution statement

Federica Recupido: Conceptualization, Methodology, Writing – original draft, Writing – review & editing. **Giuseppe C. Lama:** Conceptualization, Methodology, Writing – original draft, Writing – review & editing, Investigation, Data curation, Validation, Figures and Graphical Abstract, Conceptualization. **Mario Ammendola:** Investigation, data analysis. **Ferdinando De Luca Bossa:** Investigation, data analysis. **Andrea Minigher:** Formal analysis, Methodology. **Pietro Campaner:** Formal analysis, Methodology. **Angela Gala Morena:** Lignocellulosic preparation, characterization, Data curation, Writing – original draft. **Tzanko Tzanov:** Lignocellulosic, Data curation, Writing – review & editing, Validation. **Mariana Ornelas:** Silica preparation/characterization, Data curation, Writing – original draft. **Ana Barros:** Silica preparation/characterization, Data curation, Writing – original draft. **Filipa Gomes:** Silica preparation/characterization, Data curation, Writing – original draft. **Veronica Bouça:** Silica preparation/characterization, Data curation, Writing – original draft. **Regina Malgueiro:** Silica preparation/characterization, Data curation, Writing – original draft. **Monica Sanchez:** Fire investigation, Data curation, Validation, Writing – original draft, Writing – review & editing. **Eva Martinez:** Fire investigation, Data curation, Validation, Writing – original draft, Writing – review & editing. **Luigi Sorrentino:** Mechanical, Investigation, Data curation, Validation, Figures and Graphical Abstract, Conceptualization. **Laura Boggioni:** Resources, Data curation, and reference analysis, Funding acquisition, Supervision. **Massimo Perucca:** Visualization, of environmental and market impact. **Sridhar Anegalla:** Visualization, of environmental and market impact. **Roberta Marzella:** Visualization, of environmental and market impact. **Pierluigi Moimare:** Resources, Data curation, and reference analysis. **Letizia Verdolotti:** Conceptualization, Methodology, Writing – original draft, Writing – review & editing, Resources, Funding acquisition, Supervision, All authors have read and agreed to the published version of the manuscript.

Declaration of competing interest

The authors declare that they have no known competing financial interests or personal relationships that could have appeared to influence the work reported in this paper.

Data availability

Data will be made available on request.

Acknowledgments

The authors are grateful to Fabio Docimo, Mariarosaria Marcedula and Alessandra Aldi (CNR-IPCB) for the technical support.

Appendix A. Supplementary data

Supplementary data to this article can be found online at https://doi.org/10.1016/j.polymer.2023.125674.

References

[1] F. Coccia, L. Gryshchuk, P. Moimare, F. De Luca Bossa, L. Verdolotti, L. Boggioni, G.C. Lama, Chemically functionalized nanocrystalline cellulose as active filler in polyurethane foams, Polymers 13 (2021) 2556.
[2] M. Garside, Production capacity of bioplastics worldwide from 2017 to 2024, by type, statista, January 2022, https://www.statista.com/statistics/678684/global-production-capacity-of-bioplastics-by-type/, 2020.
[3] S. Wendels, L. Avérous, Biobased polyurethanes for biomedical applications, Bioact. Mater. 6 (2021) 1083–1106.
[4] J.V. Džunuzović, I.S. Stefanović, E.S. Džunuzović, A. Dapčević, S.I. Šešlija, B. D. Balanč, G.C. Lama, Polyurethane networks based on polycaprolactone and hyperbranched polyester: structural, thermal and mechanical investigation, Prog. Org. Coating 137 (2019), 105305.
[5] C.S. Carriço, T. Fraga, V.M.D. Pasa, Production and characterization of polyurethane foams from a simple mixture of castor oil, crude glycerol and untreated lignin as bio-based polyols, Eur. Polym. J. 85 (2016) 53–61.
[6] M. Stanzione, V. Russo, M. Oliviero, L. Verdolotti, A. Sorrentino, M. Di Serio M, R. Tesser, S. Iannace, M. Lavorgna, Synthesis and characterization of sustainable polyurethane foams based on polyhydroxils with different terminal groups, Polymer 149 (2018) 134–145.
[7] J.H. Lee, S.H. Kim, K.W. Oh, Bio-based polyurethane foams with castor oil based multifunctional polyols for improved compressive properties, Polymers 13 (2021) 576.
[8] F. De Luca Bossa, C. Santillo, L. Verdolotti, P. Campaner, A. Minigher, L. Boggioni, S. Losio, S. Iannace, G.C. Lama, Greener nanocomposite polyurethane foam based on sustainable polyol and natural fillers: investigation of chemico-physical and mechanical properties, Materials 13 (2020) 211.
[9] M. Oliviero, L. Verdolotti, M. Stanzione, M. Lavorgna, S. Iannace, M. Tarello, A. Sorrentino, Bio-based flexible polyurethane foams derived from succinic polyol: mechanical and acoustic performances, J. Appl. Polym. Sci. 134 (2017), 45113.
[10] S.D. Bote, A. Kiziltas, I. Scheper, D. Mielewski, R. Narayan, Biobased flexible polyurethane foams manufactured from lactide-based polyester-ether polyols for automotive applications, App. Pol. Sci. 138 (2021), e50690.
[11] F. De Luca Bossa, L. Verdolotti, V. Russo, P. Camapaner A. Minigher, G.C. Lama, L. Boggioni, R. Tesser, M. Larvogna, Upgrading sustainable polyurethane foam based on greener polyols: succinic-based polyol and mannich-based polyol, Materials 13 (2020) 3170.
[12] G.C.F. Lama, A. Errico, V. Pasquino, S. Mirzaei, F. Preti, G.B. Chirico, Velocity uncertainty quantification based on Riparian vegetation indices in open channels colonized by *Phragmites australis*, J. Ecohydr. 7 (2022) 71.
[13] U. Cabulis, M. Kirpluks, U. Stirna, M.J. Lopez, M.d.C. Vargas-Garcia, F. Suárez-Estrella, J. Moreno, Rigid polyurethane foams obtained from tall oil and filled with natural fibers: application as a support for immobilization of lignin-degrading microorganisms, J. Cell. Plast. 48 (2012) 6.
[14] S.K. Rajanna, D. Kumar, M. Vinjamur, M. Mukhopadhyay, Silica aerogel microparticles from rice husk ash for drug delivery, Ind. Eng. Chem. Res. 54 (2015) 949–956.
[15] F. Adam, J.N. Appaturi, A. Iqbal, The utilization of rice husk silica as a catalyst: review and recent progress, Catal. Today 190 (2012) 2–14.
[16] Y. Shen, Rice husk silica-derived nanomaterials for battery applications: a literature review, J. Agric. Food Chem. 65 (2017) 995–1004.
[17] S.A. Zareei, F. Ameri, F. Dorostkar, M. Ahmadic, Rice husk ash as a partial replacement of cement in high strength concrete containing micro silica: evaluating durability and mechanical properties, Case Stud. Constr. Mater. 7 (2017) 73–81.
[18] S.K.S. Hossain, L. Mathur, P.K. Roy, Rice husk/Rice husk ash as an alternative source of silica in ceramics: a review, J. Asian Ceram. Soc. 6 (2018) 299–313.
[19] A. Moosa, B.F. Saddam, Synthesis and characterization of nanosilica from rice husk with applications to polymer composites, Am. J. Mat. Sci. 7 (2017) 223–231.
[20] C.K. Kundu, L. Song, Y. Hu, Nanoparticles based coatings for multifunctional polyamide 66 textiles with improved flame retardancy and hydrophilicity, J. Taiwan Inst. Chem. Eng. 112 (2020) 15–19.
[21] X.W. Cheng, J.P. Guan, X.H. Yang, R.C. Tang, F. Yao, Phytic acid/silica organic-inorganic hybrid sol system: a novel and durable flame retardant approach for wool fabric, J. Mater. Res. Technol. 9 (2020) 700–708.
[22] Y. Sui, L. Qu, X. Dai, P. Li, J. Zhang, S. Luo, C.A. Zhang, Green self-assembled organic supermolecule as an effective flame retardant for epoxy resin, RSC Adv. 10 (2020) 12492–12503.
[23] M.C. Andre, J.C. Hausman, G.A. Guerriero, *Cannabis sativa*: the plant of the thousand and one molecules, Front. Plant Sci. 7 (2016) 19.
[24] H.P. Vasantha Rupasinghe, A. Davis, S.K. Kumar, B. Murray, V.D. Zheljazkov, Industrial hemp (*Cannabis Sativa* subsp. Sativa) as an emerging source for value-added functional food ingredients and nutraceuticals, Molecules 25 (2020) 4078.
[25] K. Kerner, I. Jõudu, A. Tänavots, P.R. Venskutonis, Application of raw and defatted by supercritical CO_2 hemp seed press-cake and sweet grass antioxidant extract in pork burger patties, Foods 10 (2021) 1904.

[26] K. Kotecka-Majchrzak, N. Kasałka-Czarna, A. Spychaj, B. Mikołajczak, M. Montowska, The effect of hemp cake (*Cannabis Sativa l.*) on the characteristics of meatballs stored in refrigerated conditions, Molecules 26 (2021) 5284.

[27] ISO 14040, Environmental Management—Life Cycle Assessment—Principles and Framework, International Organization for Standardization, Geneva, Switzerland, 2006.

[28] ISO 14044, Environmental Management—Life Cycle Assessment—Requirements and Guidelines, International Organization for Standardization, Geneva, Switzerland, 2006.

[29] L. Ben-Alon, V. Loftness, K.A. Harries, E. Cochran Hameen, Life cycle assessment (LCA) of natural vs conventional building assemblies, Renew. Sust. Ene.r Rev. 144 (2021), 110951.

[30] A.G. Morena, I. Stefanov, K. Ivanova, S. Pérez-Rafael, M. Sánchez-Soto, T. Tzanov, Antibacterial polyurethane foams with incorporated lignin-capped silver nanoparticles for chronic wound treatment, Ind. Eng. Chem. Res. 59 (2020) 4504–4514.

[31] I.A. Gilca, V.I. Popa, C. Crestini, Obtaining lignin nanoparticles by sonication. Ultrason, Sonochem 23 (2015) 369–375.

[32] F. Recupido, M. Petala, S. Caserta, M. Kostoglou, S. Guido, T.D. Karapantsios, Wetting properties of dehydrated biofilms under different growth conditions, Col. Surf. B. Bio 210 (2022), 112245.

[33] M. Lavorgna, L. Verdolotti, B. Liguori, I. Capasso, F. Iucolano, S. Iannace, Recycling and recovery of PE-PP-PET-based fiber polymeric wastes as aggregate replacement in lightweight mortar: evaluation of environmental friendly application, Environ. Prog. Sustain. Energy 33 (2014) 1445–1451.

[34] L. Verdolotti, M. Oliviero, M. Lavorgna, C. Santillo, F. Tallia, S. Iannace, S. Chen, J. R. Jones, Aerogel-like" polysiloxane-polyurethane hybrid foams with enhanced mechanical and thermal-insulating properties, Compos. Sci. Technol. 213 (2021), 108917.

[35] Reaction-to-fire Tests-ISO 5660-1:2-002, Ignitability of Products Subjected to Direct Impingement of Flame —, Part, 1, ASTM International, 2020.

[36] Reaction-to-fire tests — ISO 5660-1:2-002, Heat Release, Smoke Production and Mass Loss Rate — Part 1: Heat Release Rate (Cone Calorimeter Method), ASTM International, 2002.

[37] ASTM D1621, Standard Test Method for Compressive Properties of Rigid Cellular Plastics, ASTM International, 2016.

[38] M.F. Ashby, L.J. Gibson, Cellular Solids: Structure and Properties, Press Syndicate of the University of Cambridge, Cambridge UK, 1997, pp. 175–231.

[39] O. Smorygo, A.A. Gokhale, A. Vazhnova, A. Stefan, Ultra-low density epoxy/polystyrene foam composite with high specific strength and pseudo-plastic behavior, Comp. Comm. 15 (2019) 64–67.

[40] R. Narasimman, S. Vijayan, K. Prabhakaran, Carbon-carbon composite foams with high specific strength from sucrose and milled carbon fiber, Mater. Lett. 144 (2015) 46–49.

[41] T. Abdulla, A. Yerokhin, R. Goodall, Effect of Plasma Electrolytic Oxidation coating on the specific strength of open-cell aluminum foams, Mater. Des. 32 (7) (2011) 3742–3749.

[42] E.M. Wouterson, F.Y. Boey, X. Hu, S.C. Wong, Specific properties and fracture toughness of syntactic foam: effect of foam microstructures, Compos. Sci. Technol. 65 (2005) 1840–1850.

[43] M. Benedetti, J. Klarin, F. Johansson, V. Fontanari, V. Luchin, G. Zappini, A. Molinari, Study of the compression behaviour of Ti_6Al_4V trabecular structures produced by additive laser manufacturing, Materials 12 (2019) 1471.

[44] J.B. Guinée, M. Gorrée, R. Heijungs, G. Huppes, R. Kleijn, A. de Koning, L. van Oers, A. Wegener Sleeswijk, S. Suh, H.A. Udo de Haes, H. de Bruijn, R. van Duin, M. A.J. Huijbregts, Handbook on Life Cycle Assessment. Operational Guide to the ISO Standards I: LCA in Perspective IIa: Guide IIb: Operational Annex III: Scientific Background, Kluwer Academic Publishers, 2002.

[45] L. Verdolotti, M. Lavorgna, E. Di Maio, S. Iannace, Hydration-induced reinforcement of rigid polyurethane–cement foams: the effect of the co-continuous morphology on the thermal-oxidative stability, Polym. Degrad. Stabil. 98 (2013) 64–72.

[46] H. Aguilar, D. Conceição, A. Barros, V. Bouça, M. Ornelas, R. Malgueiro, A. Carvalho, A. Portela, C. Silva, E. Döpelheuer, S. Grishchuk, L. Gryshchuk, M. Gilberg, B. Wetzel, Use of biogenic silica nanoparticles derived from biomass in polymeric formulations and their applications, Math. Comput. 4 (2020) 22–28.

[47] K.M. Li, J.G. Jiang, S.C. Tian, X.J. Chen, F. Yan, Influence of silica types on synthesis and performance of amine-silica hybrid materials used for CO_2 capture, J. Phys. Chem. C 118 (2014) 2454–2462.

[48] R. Zhang, S. Cai, G. Xu, H. Zhao, Y. Li, X. Wang, K. Huang, M. Ren, X. Wu, Crack self-healing of phytic acid conversion coating on AZ31 magnesium alloy by heat treatment and the corrosion resistance, Appl. Surf. Sci. 313 (2014) 896–904.

[49] K. Sykam, M. Försth, G. Sas, Á. Restás, O. Das, Phytic acid: a bio-based flame retardant for cotton and wool fabrics, Ind. Crop. Prod. 164 (2021), 113349.

[50] I. Rotaru, M. Ionescu, D. Donescu, S. Capitanu, M. Vuluga, Bis-Mannich polyether polyols with aromatic structures, Mater. Plast. 46 (2009) 21–25.

[51] X. Zhou, J. Sethi, S. Geng, L. Berglund, N. Frisk, Y. Aitomäki, M.M. Sain, K. Oksman, Dispersion and reinforcing effect of carrot nanofibers on biopolyurethane foams, Mat.Des. 110 (2016) 526–531.

[52] B. Schartel, Development of fire retarded materials –interpretation of cone calorimeter data, Fire Mater. 31 (2007) 327–354.

[53] M. Barbalini, L. Bertolla, J. Toušek, G. Malucelli, Hybrid silica-phytic acid coatings: effect on the thermal stability and flame retardancy of cotton, Polymers 11 (2019) 1664.

[54] R.V. Petrella, The assessment of full-scale fire hazards from cone calorimeter data, J. Fire Sci. 12 (1994) 14–43.

[55] H. Yang, B. Yu, P. Song, C. Maluk, H. Wang, Surface-coating engineering for flame retardant flexible polyurethane foams: a critical review, Comp. Part B 176 (2019), 107185.

[56] L. Quian, L. Li, Y. Chen, B. Xu, Y. Qiu, Quickly self-extinguishing flame retardant behavior of rigid polyurethane foams linked with phosphaphenanthrene groups, Comp. Part B 175 (2019), 107186.

[57] Y. Hu, Z. Zhou, S. Li, D. Yang, S. Zhang, Y. Hou, Flame retarded rigid polyurethane foams composites modified by aluminum diethylphosphinate and expanded graphite, Front. Mat. 7 (2021), 629284.

[58] N.V. Gama, R. Silva, F. Mohseni, A. Davarpanah, V.S. Amaral, A. Ferreira, A. Barros-Timmons, Enhancement of physical and reaction to fire properties of crude glycerol polyurethane foams filled with expanded graphite, Polym. Test. 69 (2018) 199–207.

[59] D. Antolinc, K. Eleršič Filipič, Recycling of nonwoven polyethylene terephthalate textile into thermal and acoustic insulation for more sustainable buildings, Polymers 13 (2021) 3090.

[60] U. Berardi, J. Madzarevic, Microstructural analysis and blowing agent concentration in aged polyurethane and polyisocyanurate foams, Appl. Therm. Eng. 164 (2020), 114440.

[61] T. Zhai, L. Verdolotti, S. Kacilius, P. Cerruti, G. Gentile, H. Xia, M. Stanzione, G. G. Buonocore, M. Lavorgna, High piezo-resistive performances of anisotropic composites realized by embedding rGO-based chitosan aerogels into open cell polyurethane foams, Nanoscale 11 (18) (2019) 8835.

[62] S. Członka, A. Strakowska, A. Kairyte, The impact of hemp shives impregnated with selected plant oils on mechanical, thermal, and insulating properties of polyurethane composite foams, Materials 13 (2020) 4709.

[63] U. Cabulis, I. Sevastyanova, J. Andersons, I. Beverte, Rapeseed oil-based rigid polyisocyanurate foams modified with nanoparticles of various type, Polymery /Polymers 59 (2014) 3.

[64] L. Verdolotti, E. Di Maio, M. Lavorgna, S. Iannace, Hydration-induced reinforcement of rigid polyurethane-cement foams: mechanical and functional properties, J. Mater. Sci. 47 (19) (2012) 6948.

[65] L.J. Gibson, F. Ashby, T.J. Zhang, T.C. Triantafillou, Failure surfaces for cellular materials under multiaxial loads–I. Modelling, Int. J. Mech. Sci. 31 (1989) 635–663.

[66] M.F. Ashby, The properties of foams and lattices, Phil. Trans. R. Soc. A 364 (2006) 15–30.

[67] A. Fridrihsone, F. Romagnoli, V. Kirsanovs, U. Cabulis, Life Cycle Assessment of vegetable oil based polyols for polyurethane production, J. Clean. Prod. 266 (2020), 121403.